Application of BaTiO$_3$ as anode materials for H$_2$S-containing CH$_4$ fueled solid oxide fuel cells

Jian-Hui Li, Xian-Zhu Fu, Jing-Li Luo[*], Karl T. Chuang, Alan R. Sanger

Department of Chemical and Materials Engineering, University of Alberta, Edmonton, Alberta, Canada T6G 2G6

ARTICLE INFO

ABSTRACT

Undoped BaTiO$_3$ perovskite oxide is more effective than SrTiO$_3$ and La$_2$Ti$_2$O$_7$ oxide as anode catalyst in SOFC fueled with H$_2$S-containing methane. Electrochemical performance, impedance spectroscopy and other characterizations show that pure BaTiO$_3$ is a good anode catalyst for conversion of methane in SOFC, especially in H$_2$S-containing atmospheres. Compared with SrTiO$_3$ and La$_2$Ti$_2$O$_7$ samples, the BaTiO$_3$–based fuel cell has higher resistance to carbon deposition, better electrochemical performance and much higher stability during long term operation. A maximum power density of 135 mW cm^{-2} was achieved at 900 °C with 0.5% H$_2$S–CH$_4$ in a fuel cell having a 300 μm thick YSZ electrolyte. High catalytic activity for methane conversion, mixed electronic and ionic conductivity, and the surface basicity of BaTiO$_3$ unexpectedly provides promising performance as anodes in SOFC.

© 2012 Elsevier B.V. All rights reserved.

1. Introduction

Solid oxide fuel cells (SOFCs) have the advantages of high efficiency, low pollution, simplified mechanical and operating system and other features which make them very attractive for use in energy conversion systems [1,2]. SOFCs are suitable for many stationary power generation and back-up power applications. While very advantageous from a practical perspective, currently available fuels for SOFCs usually contain deleterious contaminants such as hydrogen sulfide (H$_2$S) or carbon monoxide (CO). A corrosive and extremely toxic gas, the concentration of H$_2$S present in natural gas ranges from trace amounts to more than 80% [3]. Natural gas which contains at least 50 ppm of H$_2$S is named sour natural gas, which needs to be treated before transportation and use due to the dangerous and corrosive nature of H$_2$S. Gas processing plants convert this toxic gas into elemental sulfur and water vapor via the well-established Claus process [4].

A SOFC with H$_2$S tolerance from 500 ppm up to several vol% is highly desirable because it would be able to utilize sour natural gas directly. H$_2$S is recognized as a problem in operating conventional SOFC as it can poison typical catalysts and is corrosive [5]. The most efficient H$_2$ SOFC catalyst (Ni–YSZ) to date is poisoned by H$_2$S rapidly

either to form a sulfide or to poison the anode surface, which significantly degrades its activity for electrochemical oxidation of H$_2$ [6,7]. Therefore it is desirable to use an alternative sulfur tolerant anode material. The perovskite oxides that have mixed ionic and electronic conductivity (MIEC) are used as alternative anode materials for conversion of H$_2$S-containing feeds. Compared with metal-based anodes, such transition-metal-based perovskite oxides are less likely to promote coking or suffer from sulfur poisoning [8]. Various perovskite oxides, mostly based on doped strontium perovskite oxides, such as CeSrVO$_x$ [5], LaSrVO$_x$ [9–14], LaYSrCrO$_x$ [15], LaSrCrMnO$_x$ [16], LaSrTiO$_3$ [17,18] and YSrTiO$_3$ [19] have attracted attention as the anode materials for SOFC with H$_2$S-containing fuels since they show high electrical conductivity and chemical stability under the operating conditions. Some other double-perovskite structured materials, such as SrMgMoO$_x$ [20] or SrMgMnMoO$_x$ [21] also were considered as alternative anode materials. However, to date the electrocatalytic activity of these anode materials for SOFCs using H$_2$S-containing fuels, especially at high H$_2$S concentration, has not been applied widely.

Recently Vincent et al. found that doping of Ba into LaSrTiO$_3$ improved anode reaction activity [22]. Barium oxide based catalysts were found to be very active for the oxidation of methane, and there are many reports describing methane activation using Ba-based oxides, such as partial oxidation of methane (POM) [23,24], methane catalytic combustion [25,26], and oxidative coupling of methane (OCM) [27–29]. BaO significantly improved the catalytic

* Corresponding author. Tel.: +1 780 492 2232; fax: +1 780 492 2881.
E-mail address: jingli.luo@ualberta.ca (J.-L. Luo).

performance of Gd_2O_3 for OCM [28]. Also it was found that BaO suppressed carbon deposition at the SOFC anode when methane was the fuel [30,31]. Carbon deposition is prevented effectively during the decomposition of CH_4 due to the basicity present at the anode surface. Among these, $BaTiO_3$ (BT) has been extensively studied for both partial oxidation and combustion of methane at high temperature since BT is very active in activation of both methane and oxygen [23,24,32–34]. Besides its application as catalyst, BT also has wide application as a major material in modern electronics technology [35].

In this study, we developed a BT anode catalyst with high activity for methane conversion that is stable in hydrocarbon- and H_2S-containing feeds. The stability and electrochemical properties of BT as anode material were investigated for use in various fuels, and during extended runs with H_2S and CH_4 fuels. For comparison, two other perovskite oxides, $SrTiO_3$ (ST) and $La_2Ti_2O_7$ (LT), also were tested under the same conditions. The intrinsic differences between these catalysts are discussed.

2. Experimental

2.1. Catalyst preparation

The various catalysts were prepared by solid state synthesis from high purity powdered precursors: $BaCO_3$ (Fisher, 99.4%), $SrCO_3$ (BDH, 99%), La_2O_3 (Alfa Aesar, 99.99%), and TiO_2(BDH, 99.5%). Equimolar amounts of the powders were weighed, M:Ti (M = Ba, Sr or La), and ball milled for 15 h to mix them uniformly. The mixed powders were calcined in air at 1200 °C for 5 h. Phase purity was determined using X-ray diffraction (Siemens D5000, Ni filtered, Co Kα1). YSZ was a commercial powder (TOSHO) and used as received.

2.2. Fuel cell fabrication

Fuel cells were fabricated using commercial YSZ disks (FCM, "fuelcellmaterials.com") as electrolyte, 300 m thick and 25 mm in diameter. The anode and cathode were intimate mixtures of equal weights of YSZ with pore-precursor PMMA and with the various titanate oxide catalysts (anode), or with commercial strontium doped lanthanum manganite (LSM) powders (cathode), respectively. The mixtures were finely powdered in a planetary ball milling machine, then dispersed in glycerine to form the corresponding electrode inks. Each electrode ink was screen printed onto the opposed faces of the electrolyte to form a membrane electrode assembly (MEA) with circular 1 cm^2 anode electrodes, and then sintered 1 h at 1200 °C. After sintering the combination of anode and electrolyte, 1 cm^2 platinum paste was painted on the cathode side and gold paste was painted on the anode side, then both pastes were sintered in-situ to form current collectors. An
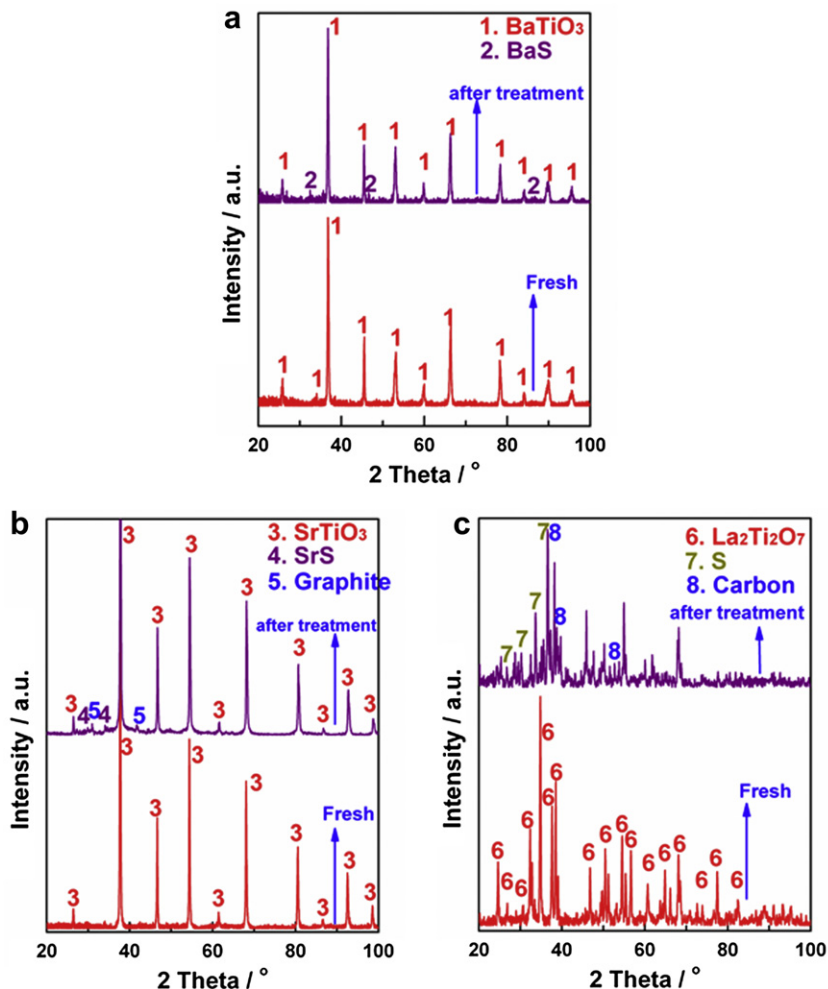

Fig. 1. XRD patterns (Ni filtered, Co Kα1) of (a) $BaTiO_3$; (b) $SrTiO_3$ and (c) $La_2Ti_2O_7$ before and after calcining in 0.5% H_2S–CH_4 at 950 °C for 10 h.

annular clear area adjacent the rim was at both sides of the electrolyte disk.

2.3. Fuel cell testing

Single cell tests were performed in a vertical furnace in a coaxial two-tube (inlet and outlet) set-up, as previously described [5]. Glass sealant (Ceramabond, Aremco Products) was used to seal the outer tube (outlet) directly to the outer edge of the anode side of the single cell electrolyte. The fuel cells were tested at each temperature, 800, 850 and 900 °C, consecutively. Anodes were reduced in-situ at 900 °C before tests. The cathode side of each membrane electrode assembly (MEA) was not sealed within a tube, and its compartment was supplied with air flowing at 75 mL min⁻¹. Methane (CH_4), methane with 0.5% hydrogen sulfide (0.5% H_2S–CH_4), hydrogen (H_2) and hydrogen with 0.5% hydrogen sulfide (0.5% H_2S–H_2) were used as fuels and fed dry at 75 mL/min. The fuels used for testing were sequenced in the following order: H_2, CH_4, 0.5% H_2S–H_2 and 0.5% H_2S–CH_4. Before measurements, the system was allowed to stabilize following each change of temperature and feed. Electrochemical properties were measured without any compensation at 10 mV/s for potentiodynamic analysis using a Solartron instrument (SI 1287).

2.4. Chemical stability testing

Chemical stability tests were conducted by treating powdered samples of anode materials in a quartz tube. The samples were heated in a stream of flowing, highly pure N_2, held at 950 °C in 0.5% H_2S–CH_4 (Praxair) for 10 h, and then cooled, again in a stream of pure N_2. The phase compositions of the fresh and treated powders were compared using XRD. The surface composition was determined using XPS.

2.5. Materials characterization

A Siemens D5000 Powder X-ray diffraction (XRD) system with a rotating anode and a Co target was used for analysis of all synthesized powders. The commercially available software Jade® was used to identify phases present in the samples.

A Vega-3 (Tescan) with EDXS detector (INCA, Oxford Instruments) emission scanning electron microscope (SEM) was used for characterizing cross-sections of MEAs. X-ray photoelectron spectroscopy (XPS) was performed on samples using a Kratos Analytical AXIS 165. A monochromated Al Kα (hv = 1486.6 eV) source was used at a power of 210 W, with a base pressure of 3×10^{-8} Pa in the analytical chamber. Nitrogen adsorption and desorption isotherms were recorded at 77 K on an automated micromeritics Tri-Star 3000 apparatus. Surface areas were calculated using the multipoint BET equation.

3. Results

3.1. Materials characterization

X-ray diffraction was used for phase and structural analyses (Fig. 1). The XRD patterns of fresh $BaTiO_3$ (BT; PDF#05-0626, Fig. 1a) and $SrTiO_3$ (ST; PDF#05-0634, Fig. 1b) showed that those as-prepared materials possessed perovskite structures with a cubic unit cell. However, the fresh $La_2Ti_2O_7$ catalyst had a layered perovskite structure (LT, PDF#27-1182, Fig. 1c) with a monoclinic unit cell, and did not form a $LaTiO_3$ phase. No secondary phase was detected for these samples. The BET surface areas of those samples were low, around 1.0 m²/g, a typical value for perovskite-type oxides and especially for those prepared from solid state reactions.

Scanning electron microscopic (SEM) studies were carried out to determine the morphology of catalysts and MEAs. Fig. 2a shows a SEM image of fresh $BaTiO_3$ catalyst. The large particles formed by aggregation of smaller grains with particle size 0.5–1 μm Fig. 2b shows a cross-section SEM image of an MEA made from the mixture of YSZ and BT. The thicknesses of the anode and cathode porous layers were about 40 and 20 μm, respectively.

3.2. Chemical stability tests

Chemical stability tests were performed to determine the carbon and sulfur tolerance of the various catalysts in 0.5% H_2S–CH_4 at temperatures as high as 950 °C for 10 h. XRD analyses conducted on the three samples before and after the chemical stability tests are shown in Fig. 1. Treated BT and ST retained the structure of the fresh materials; however, trace amounts of BaS and SrS, respectively, also were detected in the H_2S concentration as high as 5000 ppm. The extent of reaction of Ba(Sr)TiO_3 with H_2S to form BaS(SrS) and TiO_2 [36] was relatively low since the peaks for BaS or SrS were small and no TiO_2 peak was detected. No discernable amounts of deposited carbon were present on the tested BT sample, in contrast to ST which exhibited a graphite (PDF#
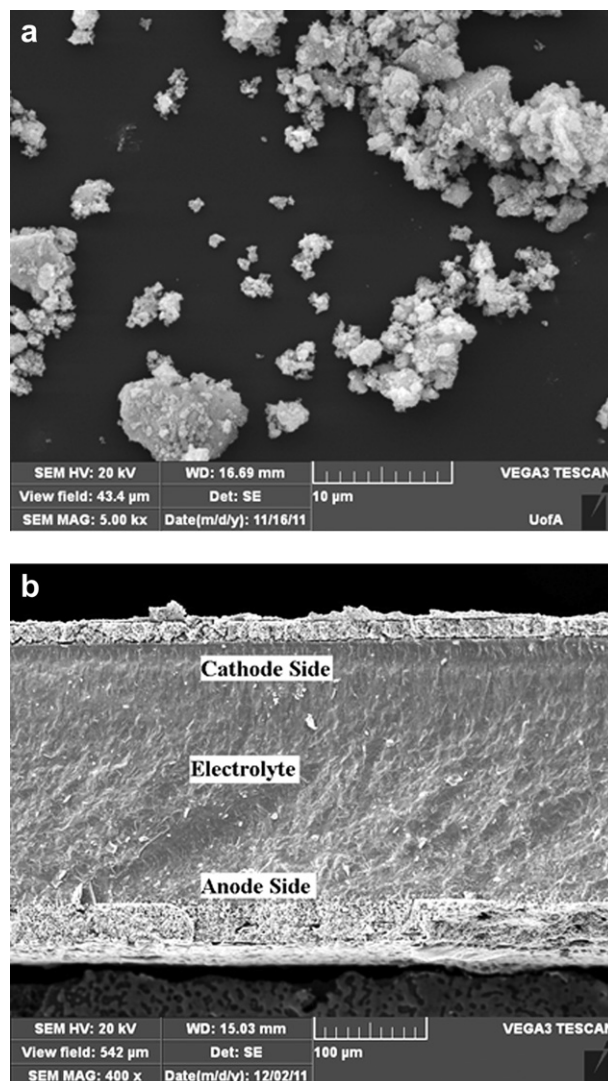
Fig. 2. SEM images of: (a) as-prepared $BaTiO_3$ particles; (b) cross-sectional view of $BaTiO_3$– based cell.
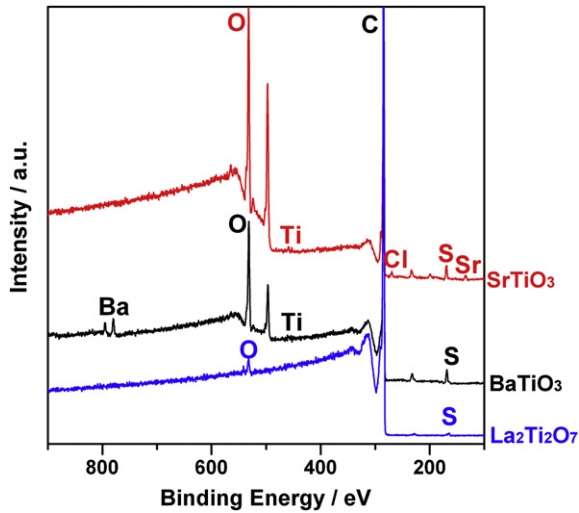
Fig. 3. XPS spectra for various anode catalysts after calcining in 0.5% H_2S–CH_4 at 950 °C for 10 h.

08-0415) peak ascribed to methane decomposition at high temperature [5]. However, the situation for LT was much more complex. The layered perovskite structure was destroyed and amounts of sulfur (PDF# 01-0478) and carbon (PDF# 46-0943) were detected on the surface. The XRD results after chemical stability tests showed the high resistance of BT to carbon deposition, in contrast to ST, LT, and previously reported $CeSrVO_x$ ($x = 3,4$) [5].

XPS (Fig. 3) characterizations were used to determine the near-surface composition and near-surface ion electronic states of the various elements after chemical stability tests. All of S, C, O, Ti and Ba (or Sr) were present in the spectra of BT(ST), while only C and traces of O and S were found in the spectrum of LT. All the XPS and XRD results showed that BT is a carbon and sulfur tolerant catalyst, while LT is not stable in H_2S- and CH_4- containing atmosphere at high temperature.

3.3. Electrochemical performance

Potentialdynamic tests were conducted to determine the electrochemical activity of the anode material for conversion of each of methane and H_2S. The MEAs were tested separately at 900, 850 and 800 °C using the following feeds: pure H_2, pure CH_4, 0.5% H_2S–H_2 and 0.5% H_2S–CH_4, in the same sequence as listed above. All the electrochemical data were obtained after stabilization of each system following change of any parameter. Fig. 4 compares the peak power densities for the three anode catalysts at different temperatures and using different feeds. In pure H_2 (Fig. 4a), the electrochemical activities were similar, and were poor, for all three anodes. However, the performances were enhanced for BT when 5000 ppm H_2S was added to the feeds (Fig. 4c). The performance in pure methane fuel over BT is better than that over ST or LT (Fig. 4b). Considerable, obvious improvements in power densities were observed for all three anodes when there was 5000 ppm H_2S in CH_4. All data show that BT exhibited a better (or at least equal) performance than either ST or LT under all test conditions, and especially when the feeds were pure methane or 0.5% H_2S–H_2.

Detailed I–V and I–P curves for the three cells using 0.5% H_2S–CH_4 as feed are compared in Fig. 5. As expected, the peak power density improved as temperature increased from 800 to 900 °C. For BT-based cell, when the fuel was 0.5% H_2S–CH_4 the maximum power density increased to 135 mW/cm² at 900 °C (Fig. 5a), about six times higher than for pure methane. The
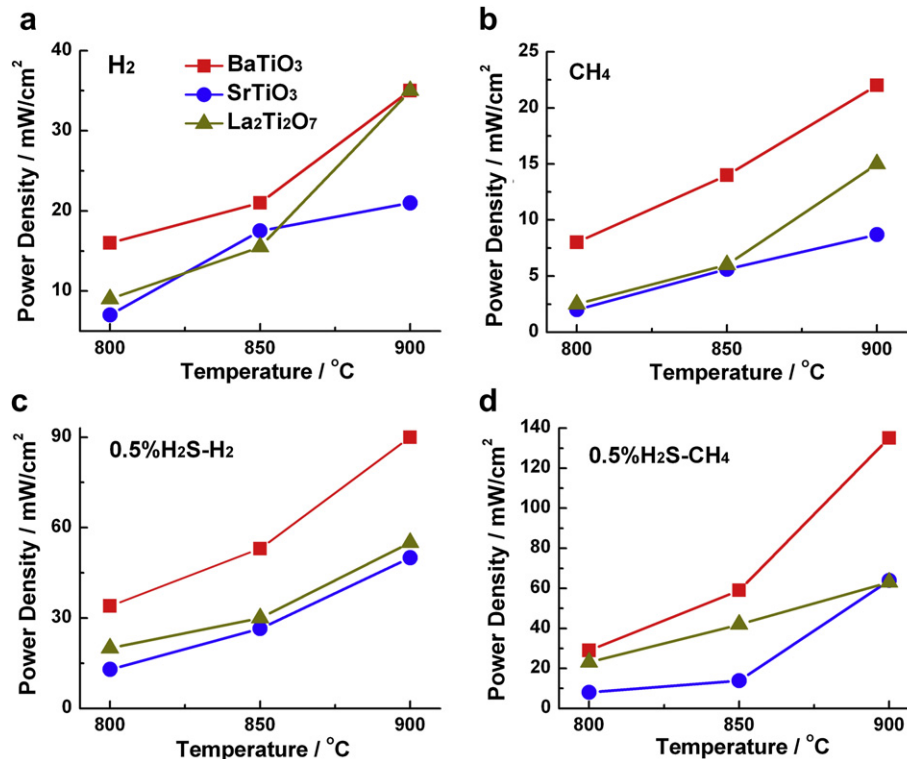

Fig. 4. Current density-voltage and power density curves for the cells with different fuels: (a) H_2; (b) CH_4; (c) 0.5% H_2S–H_2 and (d) 0.5% H_2S–CH_4 as anode feed at different temperatures.

electrochemical performances are strongly affected by reaction temperature, thus decreasing significantly as reducing temperature, especially for ST-based cell. This may be due to the lower conductivity for the samples at lower temperature. There was a strong mass transfer over-potential for BT-based cell at higher current densities, which may be attributable to limited diffusion toward the active surface for the present anode.

It is very interesting that the performance over all the anode catalysts initially was much better for the first run than when the system had stabilized, especially for BT samples. Fig. 6 shows the I–V and I–P curves for the first and second runs, and compares them with performance after stabilization, for the BT-based fuel cell using 0.5% H$_2$S–CH$_4$ at 900 °C. The performance initially declined with time on stream, and then stabilized. The peak power density for the first run reached 277 mW cm^{-2}, almost double the value after stabilization. There are two bends for all the curves. The first bends for the first and second runs are located at about 500 and 350 mA/cm^2, respectively. It decreased to about 100 mA cm^{-2} and was not very obviously for the stable run. It has been proposed that [17], the surface of the electro-catalyst becomes partly or totally covered with a layer of sulfur before running a cell. Carbon species will also be formed on the pellet surface in the decomposition of CH$_4$ activated by BaTiO$_3$, as discussed later. Therefore, the surface is covered with both carbon and sulfur species before running the test. The broad bends for the first and second runs may be attributed to the oxidation of accumulated carbon and sulfur on the surface. The significantly decrease of power density at higher current density may be due to reduced amount of accumulated carbon and sulfur, as well as limited supply of oxygen anions transferring from cathode side through the thick electrolyte. The unobvious bend for the stable run might be due to the almost run-out of the accumulated carbon and sulfur. It is obvious that there is a strong mass transfer over-potential at higher current densities for the stable run.

The corresponding impedance spectra under the open-circuit condition using 0.5% H$_2$S–CH$_4$ fuel at different temperatures, and
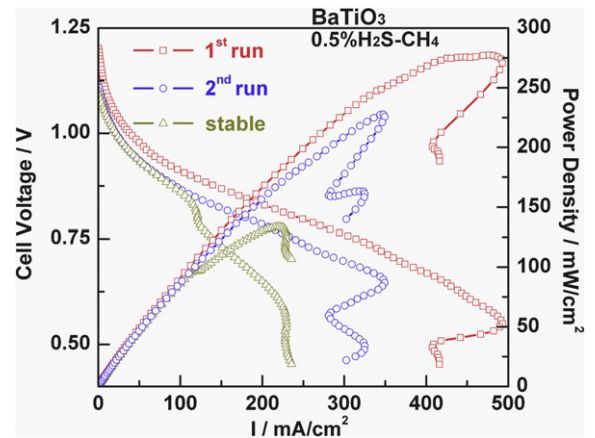

Fig. 6. Current density-voltage and power density curves as a function of time on stream for a BaTiO$_3$− based cell with 0.5% H$_2$S–CH$_4$ as anode feed.

for different fuels at 850 °C, are each compared in Fig. 7. These spectra were measured after stabilizing the cell performance. All the impedance curves showed low ohmic resistance and relatively high polarization resistance. The ohmic resistances (high frequency intercept) for each of the cells was similar. The slightly higher resistance of the LT sample was attributed to partial decomposition of LT oxide since LT was not stable in H$_2$S and CH$_4$ atmosphere, as shown in the chemical stability tests. The polarization resistance for ST appeared to be much higher than for BT and LT anodes, in agreement with the I–P results. Both ohmic and polarization resistance were reduced as the temperature was increased. Although the electronic conductivity for BT is relatively low (about 0.01 S/cm for P$_{O2}$ 10^{-15} atm at 900 °C [37]), the ohmic resistance also is low for the thin layer of BT-YSZ anode.

Fig. 8a shows the stability of performance of the catalysts in 0.5% H$_2$S–CH$_4$ over a 20 h period at 850 °C when the potential was held
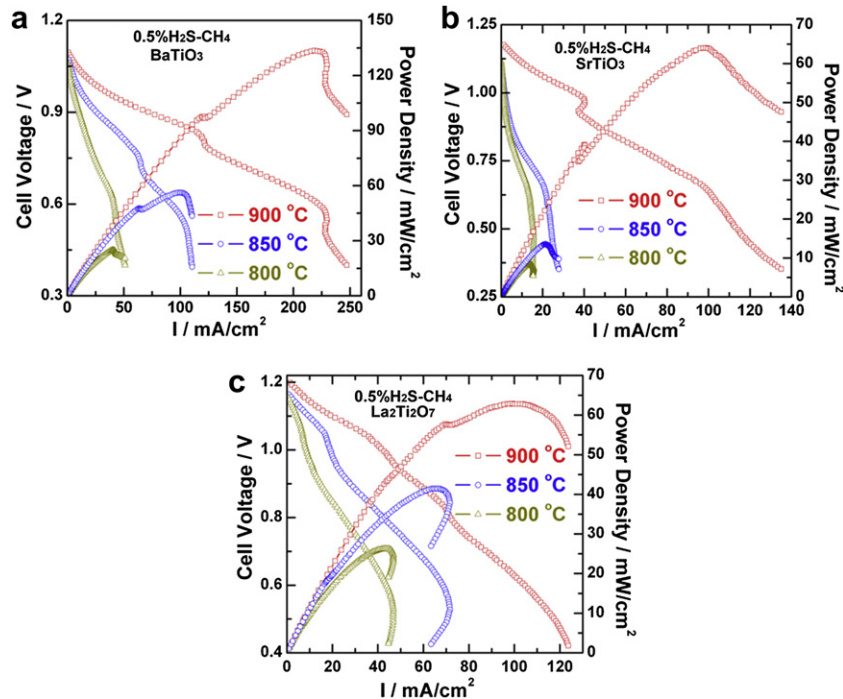

Fig. 5. Current density-voltage and power density curves at different temperatures for: (a) BaTiO$_3$; (b) SrTiO$_3$ and (c) La$_2$Ti$_2$O$_7$ fuel cells with 0.5% H$_2$S–CH$_4$.
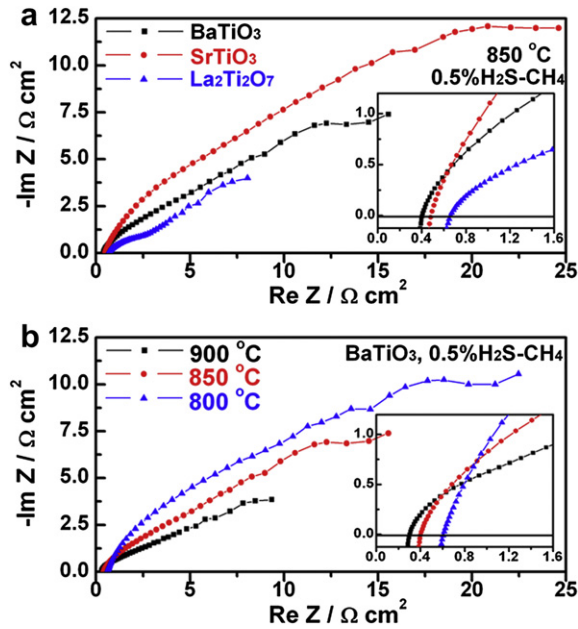
Fig. 7. Impedance spectra of: (a) the various cells fueled with 0.5% H_2S–CH_4 at 850 °C; (b) $BaTiO_3$– based cell fueled with 0.5% H_2S–CH_4 at different temperatures.

at 0.7 V. There was a rapid degradation in current density and power density for ST and LT anodes, in contrast to BT which showed an increase under the same testing conditions. When the holding potential was decreased to 0.6 V (Fig. 8b), the power density also increased slightly. There was no degradation of BT during almost 100 h operation at either 0.6 or 0.7 V. It took longer to stabilize the performance when the potential was held at 0.6 V than at 0.7 V.

3.4. Characterization of the anode after reaction

The anode feed was shifted to pure H_2 immediately after the electrochemical stability test was finished, and the temperature then was decreased to room temperature at 2.5 °C/min. SEM and EDX were used to characterize the MEAs after reaction. Fig. 9 shows cross-sectional views of the anode and cathode sides of a BT-based fuel cell. It is clear that the materials had not decomposed and that interfaces between BT-YSZ or LSM-YSZ each retained good contact and good adhesion.

The SEM images of the selected anode surfaces for a BT cell, as an example, are shown in Fig. 9c. It can be seen that the anode was overlayered with highly porous gold current collector. EDX characterizations were performed at two selected points for each cell.

Taking BT-based cell as an example which indicated in Fig. 9c, Point 1 was on the BT-YSZ surface, while point 2 was on the gold paste surface. Results for the various anode surfaces after electrochemical test are shown in Fig. 10. M (M = Ba, Sr or La, respectively), Ti, O, Zr, Y (trace), C and S were all present at point 1 for each sample, showing that the catalyst components were well mixed and well distributed. There are a great number of C and S on the gold paste surface for each cell, which indicate that methane can be decompose on the whole anode surface at the high reaction temperature and the cracked carbon was deposited on the anode surface.

4. Discussion

Perovskite $BaTiO_3$ was investigated as anode catalyst for SOFC using H_2 or CH_4 feeds, with and without 5000 ppm H_2S, and compared with performance of $SrTiO_3$ or $La_2Ti_2O_7$ based anode catalysts. The BT catalyst proved to be a much more carbon and sulfur tolerant material under SOFC operating conditions, active for methane oxidation, and achieved stable power density of 135 mW cm^{-2} in 0.5% H_2S–CH_4 at 900 °C in a fuel cell with a 300 μm thick YSZ electrolyte. To the best of our knowledge, this is the first time to date that this simple and typical perovskite oxide was used as anode catalyst for conversion of feeds containing both H_2S and methane.

The stable power density achieved was significantly higher than that using previously described anode catalysts $La_{0.4}Sr_{0.45}Ba_{0.15}TiO_3$ [22] and $Ce_{0.9}Sr_{0.1}VO_3$ [5]. In comparison with the ST and LT anodes prepared in the same manner, the BT catalyst showed much higher electrochemical performance under the majority of testing conditions, and better stability and resistance to carbon deposition and sulfur poisoning. Based on comparisons of electrochemical performance and catalyst characterizations, the great differences in catalytic behavior of the catalysts are attributed to several important distinctions in the properties of BT oxides.

It is well known that an SOFC generates electricity through the reduction of O_2 to O^{2-} anions at the cathode side, transfer of the anions through an ion conducting and electronic insulator electrolyte (herein commonly used YSZ), and finally by the oxidation of the fuel with O^{2-} anions at the anode side, with release of electrons [38]. The anode must be an ionic and electronic conductor, and also a catalyst for oxidation of the fuel by O^{2-} anions. Therefore, the anode should satisfy several important requirements: i.e. thermodynamically stable under anode operating conditions, catalytically active, electronically and ionically conductive, and chemically inert when in contact with electrolyte and interconnect [39]. The Ni particles in the classic Ni/YSZ cermet anode serve as an excellent catalyst and electron conduction, but react with H_2S. Undoped $BaTiO_3$ is a nonstoichiometric compound which possesses a mixed ionic and electronic conductivity throughout an extended range of
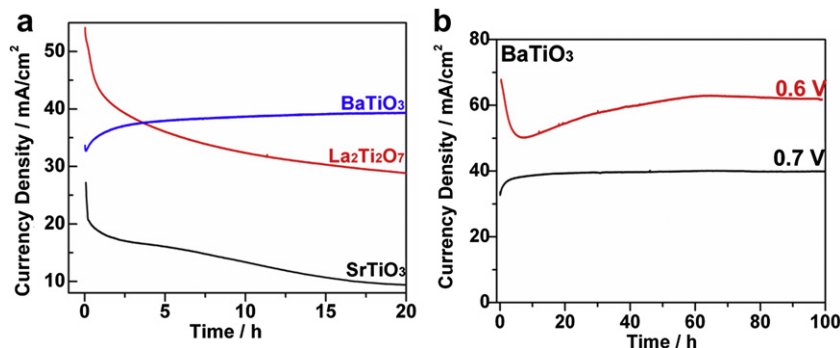

Fig. 8. The current density as a function of time with 0.5% H_2S–CH_4 at 850 °C, holding the cell potential at: (a) 0.7 V for different cells and (b) at 0.6 or 0.7 V for $BaTiO_3$– based cell.

oxygen partial pressures at high temperature. Three mass transport paths (the oxide ion conduction path, the electron conducting path and the gas diffusion path) are required to enable a porous BT anode catalyst to access oxide ions, electrons and fuel in the SOFC system.

4.1. Catalytic activity

During the electrochemical tests we found that the performance for the first run was much better than subsequent runs, and decreased gradually to reach stable performance for the following runs (Fig. 6). To gain insight into the reason for this phenomenon, the $I-V$ and $I-P$ curves were determined as a function of interval

Fig. 9. SEM images of a $BaTiO_3-$ based fuel cell after electrochemical testing: (a) anode side and (b) cathode side; (c) the selected area for EDX characterization (Point 1 and Point 2 were selected to perform EDX characterization).

time between each run for a BT-based cell fueled with 0.5% H_2S-CH_4 at 900 °C (Fig. 11). It was clear that the peak power density increased with increase in the length of the interval time between tests, and the maximum power density was about 200 mW cm^{-2} when the interval time was 10 min. It is known that methane decomposes over $BaTiO_3$ at high temperature [23]. There was about 40% conversion for partial oxidation of CH_4 into synthesis gas at 750 °C over pure $BaTiO_3$, which was comparable to the performance over the 10% Ni-doped perovskite material [24]. The first step in the CH_4 decomposition is mainly the dissociation of the C−H bond to form carbon species on the pellet surface. When the fuel cell was operated at OCV, no current was produced, thus there was no O^{2-} anion transfer through the electrolyte to the anode side. Under these conditions the deposited carbon species accumulated on the anode surface, and the accumulated amount increased with length of the interval time. Thus those carbon species that would be oxidized to CO_x and co-produce electricity
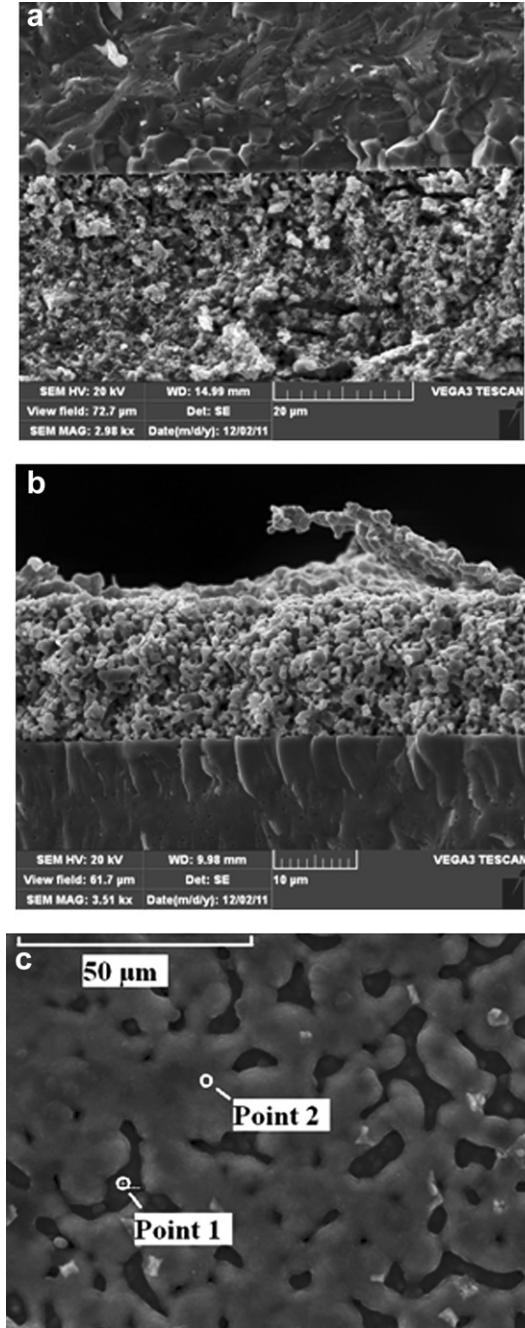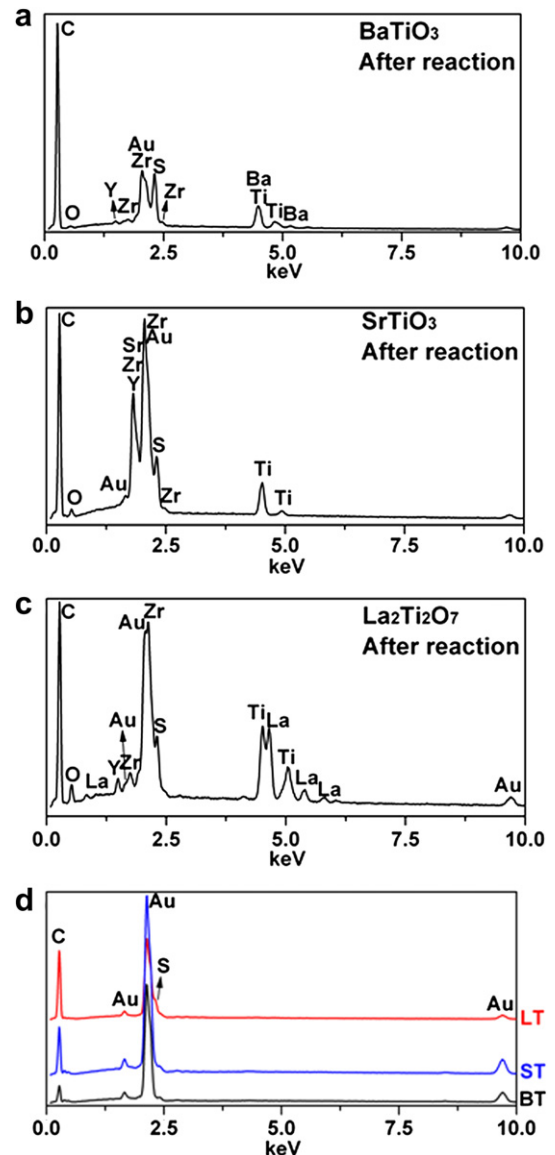

Fig. 10. EDX spectra of the various anode catalyst: (a) BT; (b) ST; (c) LT performed over MT-YSZ surface (see Point 1 in Fig. 9c) and (d) three samples over the gold paste surface (see Point 2 in Fig. 9c).
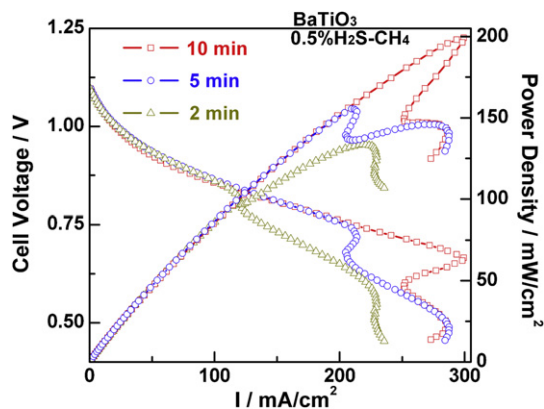
Fig. 11. Current density-voltage and power density curves as a function of waiting interval time between each test for the $BaTiO_3-$ based cell the run times with 0.5% H_2S-CH_4.

when the cell was operated at significant current density did not react at OCV.

It is proposed that alkane activation was initiated through hydrogen abstraction from CH_4 by the lattice oxygen species to form methyl radicals and finally carbon, even in the absence of additional oxygen. Lattice oxygen species in $BaTiO_3$ play an important role in such catalytic process. Perovskite-type oxide, such as $BaTiO_3$, are known to catalyze methane activation and oxidation at high temperature using lattice oxygen species [23,32–34]. Oxygen vacancies were formed during the consumption of lattice oxygen, as well as formed to achieve the overall neutrality during partially reduction of Ti^{4+} to Ti^{3+} in reducing atmosphere [40]. The density of oxygen vacancies was reduced by the immigration of O^{2-} anions from cathode. Therefore, the process is a Mars–Van Krevelen type of mechanism [41], similar to that proposed by Sohrabi et al. [42] who studied the kinetics of OCM over $CaTiO_3$ catalyst at low oxygen partial pressures (less than 0.053 bar).

4.2. Conductivity

BT is renowned for its useful electrical properties, such as ferroelectricity, piezoelectricity and a high relative permittivity, giving it a role in a wide range of applications [43]. The processing of undoped BT under reducing conditions at high temperature results in formation of oxygen deficiencies and induces semiconductivity arising from partial reduction of Ti^{4+} to Ti^{3+} ions. The lattice imperfections in the present reduced BT crystals are assumed to be oxygen vacancies. The formation of an oxygen vacancy in a BT crystal affords two electrons to maintain lattice charge neutrality.

High electronic conductivity is required in the thick anode substrate to avoid significant ohmic losses, However, it has been proposed that a 10 μm thick anode functional layer needs only a modest electronic conductivity to function effectively [44]. Recently it was demonstrated [44] that mixed ionic/electronic conductors with good ionic conductivity but only modest electronic conductivity exhibit much better electrocatalytic activity for H_2 oxidation than those electronic conductors with negligible ionic conductivity. BT is a mixed ionic and electronic conductor (MIEC) throughout an extended range of oxygen partial pressure ($10^{-15} \leq P_{O2}/atm \leq 1$); the electronic ($e^-$) and ionic ($O^{2-}$) conductivity are at least 0.01 S/cm and 7×10^{-5} S/cm at 900 °C, respectively [37,45]. This type of electron/hole/ion mixed conduction is relatively rare among binary oxides. Although the electronic conductivity for BT is relatively low, the ohmic resistance also is low for thin layers of BT-YSZ anode. Use of mixed electronic and ionic conductors extends the area in which electrochemical reactions occur to the entire electrode-gas interfacial area.

4.3. Basicity

BT exhibits a strong resistance to carbon deposition, as shown by the chemical stability tests. Such stability against carbon deposition can be related to the relatively strong basicity derived from the barium. Carbon deposition is prevented effectively during the reaction of CO_2 with CH_4 by doping of barium into a supporting Ni anode [30]. In humidified or dry reforming processes the basicity of the supporting oxide is essential for avoiding the formation of carbon deposits whereas, as is well known, large carbon deposit formations occur onto Ni supported on acidic oxides such as SiO_2 and Al_2O_3 [46]. For catalysts containing alkaline earth oxides, catalytic performance increases with increase in basicity of the alkaline earth oxides: $MgO < CaO < SrO < BaO$ [47]. The amount of electrophilic species is minimized in the presence of barium, thereby decreasing the surface acidity of the catalysts, and weakening their capability to retain a concentration of methyl/carbon species on the surface sites. Thus the basicity arising from incorporation of Ba(Sr) is ascribed as the cause of stronger resistance to carbon deposition. Hence it is ascribed the greater deposition of carbon on LT to lower basicity, as La has lower basicity than either Ba or Sr.

However, though the catalytic activity and chemical stability for BT are strong, the conductivity of BT is much less than that of doped strontium titanate materials such as LST or YST. The electrochemical performance for $BaTiO_3$–YSZ based cell is relative poor compared with that reached by other LSGM electrolyte cells with anodes such as the double perovskites Sr_2MgMoO_6 [20] or $SrMgMnMoO_x$ [21] using methane with low H_2S as the fuel. It is worth to mention that we used the electrolyte-supported cell and the thickness of the YSZ is 300 μm. In addition, YSZ has lower ionic conductivity than LSGM, especially at lower temperature. Since BT is flexible in doping with other metal cation with higher or lower valence, it is possible to enhance its conductivity, both in electronic and ionic immigration. It is also expected to enhance the electrochemical performance when other component with higher electronic conductivity is added to the anode or when the particle size of BT is decreased.

5. Conclusions

Undoped $BaTiO_3$ perovskite oxide, prepared using solid state method, is an active and stable anode catalytic material in SOFC fueled with CH_4 or H_2, and especially when containing 5000 ppm H_2S. BT catalyst shows high resistance to both carbon deposition and sulfur poisoning. Compared with $SrTiO_3$ and $La_2Ti_2O_7$ as anodes, BT-based fuel cells produce higher power density, and have much better stability during long term tests. A maximum power density of 135 mW cm^{-2} was achieved at 900 °C in 0.5% H_2S-CH_4 in a fuel cell having a 300 μm thick YSZ electrolyte, which is much better than that over the previously described anode $La_{0.4}Sr_{0.45-}Ba_{0.15}TiO_3$ and the same electrolyte. The promising catalytic behavior of BT samples is attributed to its distinct properties, including high catalytic activity for methane decomposition, mixed electronic and ionic conductivity, and high surface basicity.

References

[1] Q.M. Nguyen, T. Takahashi, Science and Technology of Ceramic Fuel Cells, Elsevier Science Ltd., 1995.
[2] S.C. Singhal, K. Kendall, High Temperature Solid Oxide Fuel Cells: Fundamentals, Design, and Applications, Elsevier Science Ltd., 2003.
[3] M. Liu, G.L. Wei, J.L. Luo, A.R. Sanger, K.T. Chuang, J. Electrochem. Soc. 150 (2003) A1025–A1029.
[4] J. Zaman, A. Chakma, Fuel Process. Tech. 41 (1995) 159.
[5] N. Danilovic, J.L. Luo, K.T. Chuang, A.R. Sanger, J. Power Sources 192 (2009) 247–257.
[6] C. Xu, J.W. Zondlo, M. Gong, F.E. Blancas, X. Liu, I.B. Celik, J. Power Sources 195 (2010) 4583–4592.
[7] M. Gong, X. Liu, J. Trembly, J. Power Sources 168 (2007) 289–298.
[8] R.J. Kee, H. Zhu, D.G. Goodwin, P. Combust. Inst. 30 (2005) 2379–2404.
[9] L. Aguilar, S.W. Zha, Z. Cheng, J. Winnick, M.L. Liu, J. Power Sources 135 (2004) 17–24.
[10] L. Aguilar, S.W. Zha, S.W. Li, J. Winnick, M. Liu, Electrochem. Solid State Lett. 7 (2004) A324–A326.
[11] Z. Cheng, S.W. Zha, L. Aguilar, M.L. Liu, Solid State Ionics 176 (2005) 1921–1928.
[12] Z. Cheng, S.W. Zha, L. Aguilar, D. Wang, J. Winnick, M.L. Liu, Electrochem. Solid State Lett. 9 (2006) A31–A33.
[13] M. Cooper, K. Channa, R. De Silva, D.J. Bayless, J. Electrochem. Soc. 157 (2010) B1713–B1718.
[14] C. Peng, J.L. Luo, A.R. Sanger, K.T. Chuang, Chem. Mat. 22 (2010) 1032–1037.
[15] X.F. Zhu, Q. Zhong, X.J. Zhao, H. Yan, Appl. Surf. Sci. 257 (2011) 1967–1971.
[16] X.J. Chen, Q.L. Liu, S.H. Chan, N.P. Brandon, K.A. Khor, J. Electrochem. Soc. 154 (2007) B1210.
[17] A.L. Vincent, J.L. Luo, K.T. Chuang, A.R. Sanger, Appl. Catal. B: Env. 106 (2011) 114–122.
[18] R. Mukundan, E.L. Brosha, F.H. Garzon, Electrochem. Solid State Lett. 7 (2004) A5–A7.
[19] H. Kurokawa, L.M. Yang, C.P. Jacobson, L.C. De Jonghe, S.J. Visco, J. Power Sources 164 (2007) 510–518.
[20] Y.H. Huang, R.I. Dass, J.C. Denyszyn, J.B. Goodenough, J. Electrochem. Soc. 153 (2006) A1266–A1272.
[21] Y.H. Huang, R.I. Dass, Z.L. Xing, J.B. Goodenough, Science 312 (2006) 254–257.
[22] A. Vincent, J.L. Luo, K.T. Chuang, A.R. Sanger, J. Power Sources 195 (2010) 769–774.
[23] A. Ogata, K. Mizuno, S. Kushiyama, T. Yamamoto, Plasma Chem. Plasma P. 18 (1998) 363–373.
[24] R. Shiozaki, A.G. Andersen, T. Hayakawa, S. Hamakawa, K. Suzuki, M. Shimizu, K. Takehira, J. Chem. Soc. Faraday Trans. 93 (1997) 3235–3242.
[25] I. Popescu, A. Urda, T. Yuzhakova, I.C. Marcu, J. Kovacs, I. Sandulescu, C. R. Chim. 12 (2009) 1072–1078.
[26] I. Popescu, I. Sandulescu, A. Redey, I.C. Marcu, Catal. Lett. 141 (2011) 445–451.
[27] M. Khodadadian, M. Taghizadeh, M. Hamidzadeh, Fuel Process. Technol. 92 (2011) 1164–1168.
[28] C.T. Au, K.D. Chen, C.F. Ng, Appl. Catal. A: Gen. 170 (1998) 81–92.
[29] M. Teymouri, E. Bagherzadeh, C. Petit, J.L. Rehspringer, S. Libs, A. Kiennemann, J. Mater. Sci. 30 (1995) 3005–3009.
[30] D.L. Rosa, A. Sin, M.L. Faro, G. Monforte, V. Antonucci, A.S. Arico, J. Power Sources 193 (2009) 160–164.
[31] L. Yang, Y. Choi, W. QinW, H. Chen, K. Blinn, M. Liu, P. Liu, J. Bai, T.A. Tyson, M. Liu, Nat. Commun. 2 (2011) 357.
[32] T. Shimizu, Catal. Rev. Sci. Eng. 34 (1992) 355–371.
[33] H. Nagamoto, K. Amanuma, H. Nobutomo, H. Inoue, Chem. Lett. (1988) 237–240.
[34] H. Arai, T. Yamada, K. Eguchi, T. Seiyama, Appl. Catal. 26 (1986) 265–276.
[35] C.R. Song, H.I. Yoo, Solid State Ionics 120 (1999) 141–153.
[36] J.X. Li, J.L. Luo, K.T. Chuang, A.R. Sanger, Electrochim. Acta 53 (2008) 3701–3707.
[37] H.I. Yoo, C.R. Song, D.K. Lee, J. Electroceram. 8 (2002) 5–36.
[38] R.J. Gorte, H. Kim, J.M. Vohs, J. Power Sources 106 (2002) 10–15.
[39] T. Kolodiazhnyi, A. Petric, J. Electroceramics 15 (2005) 5–11.
[40] W. Heywang, J. Mater. Sci. 6 (1971) 1214–1224.
[41] P. Mars, D.W.V. Krevelen, Chem. Eng. Sci. 3 (1954) 41–59.
[42] M. Sohrabi, B. Dabir, A. Eskandari, R.D. Golpasha, J. Chem. Tech. Biotechnol. 67 (1996) 15.
[43] J.A. Dawson, C.L. Freeman, L.B. Ben, J.H. Harding, D.C. Sinclair, J. Appl. Phys. 109 (2011) 084102.
[44] Q.X. Fu, F. Tietz, Fuel Cells 8 (2008) 283–293.
[45] H.I. Yoo, C.R. Song, J. Electroceramics 6 (2001) 61–74.
[46] A.P.E. York, T.C. Xiao, M.L.H. Green, Catal. Rev. 49 (2007) 511.
[47] A.M. Maitra, I. Campbell, R.J. Tyler, Appl. Catal. 85 (1992) 27.